Linking cavitation collapse energy with the erosion incubation period

Gina M. Magnotti*[1], Michele Battistoni[2], Kaushik Saha[3], Sibendu Som[1]
[1]Energy Systems Division, Argonne National Laboratory, Lemont, IL, USA
[2]Department of Engineering, Università degli Studi di Perugia, Perugia, Italy
[3]Center for Energy Studies, Indian Institute of Technology Delhi, Hauz Khas New Delhi, India
*Corresponding author: gmagnotti@anl.gov

Abstract
Cavitation-induced erosion is the result of repeated impacts from cavitation collapse events on a solid surface. To improve representation of the incubation period before material rupture within multiphase flow simulations, a new physics-based metric was derived based on cumulative energy absorbed by the solid material from repeated hydrodynamic impacts. Previous work by the authors validated the modeling framework through comparison of critical erosion sites and relative erosion severity with available experimental data. In this study, the predictive capabilities of the cavitation erosion metric are extended by relating the predicted stored energy with the solid material properties to estimate the incubation period. To extend the rigor of validation of the erosion predictions, the turbulent multiphase flow development was simulated over a range of Reynolds (Re = 1.5-$2.0·10^5$) and cavitation number (K = 1.60-1.78) conditions in an aluminum channel geometry featuring a sharp inlet corner to promote cavitation. The multiphase flow within the channel was modeled using a compressible mixture model, where phase change was represented with the Homogeneous Relaxation Model (HRM) and the turbulent flow evolution was modeled using a dynamic structure approach for Large Eddy Simulations (LES). When the average peak pressure was related to the incubation period, the incubation period and its sensitivity to changes in flow conditions was found to be overpredicted. In contrast, using the stored energy metric, multiphase flow simulations demonstrated accurate representation of the sensitivity of erosion severity to changes in flow conditions, and quantitative agreement of the predicted incubation period within 2% of the experimentally measured incubation period.

Keywords
Cavitation-induced erosion; large eddy simulation; homogeneous relaxation model

Introduction
To comply with regulation standards, direct fuel injection has been trending towards increased injection pressure of common-rail fueling technologies, with many fuel pressure systems in excess of 2000 bar. While these strategies offer emissions and fuel economy benefits, there are several challenges associated with these systems. In particular, it is well known that cavitation-induced damage in fuel injectors caused by these increased injection pressures can change the performance and hence the reliability of the engine after only several thousand hours of operation [1]. However, accurate prediction of cavitation-induced erosion has presented a technical challenge to both the engine and multiphase flow research community at large. Although there have been numerous experimental [2]-[6] and computational studies [6]-[11] to better understand the physical mechanisms governing cavitation-induced erosion, uncertainty still exists in the best way to link multiphase flow model predictions with erosion potential. Although several cavitation erosion indicators have been proposed in the literature [7]-[10],[12] no single metric has been identified as universally applicable across all injector geometries and injection conditions. The mean depth penetration rate (MDPR) parameter [12] is one of the few metrics in the literature that provides a detailed treatment of the material response to hydrodynamic impacts, as illustrated in Figure 1(a). Based on the average stress loading, σ, from repeated cavitation collapse events, the progress towards material rupture can be related to the work done on the material, W, by integrating the stress-strain curve and accounting for strain hardening effects. Erosion is related to multiphase flow predictions by equating σ with the predicted mean impact pressure, $\bar{P}$. Although MDPR is able to capture the impact of material properties on erosion risk, the simplified representation of the cloud collapse event may limit its ability to predict erosion severity over a wide range of flow conditions. In particular, using the MDPR approach, collapse events with higher impact pressures are predicted to be more erosive than impacts with lower impact pressures. However, it stands to reason that a smaller load applied for a sufficiently long period of time could be more erosive than a large load applied over a short duration. It is therefore clear that the influence of impact loading time scale on erosion severity cannot be captured by the MDPR approach.
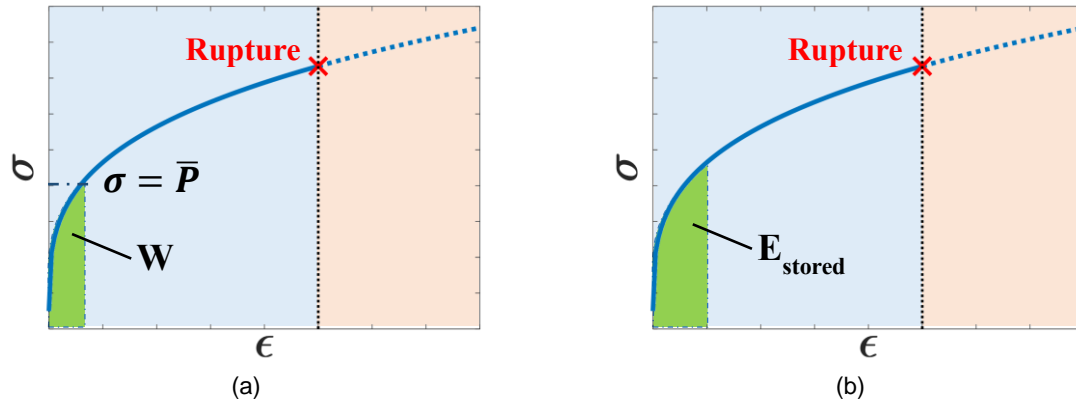
Figure 1. Schematic of the engineering stress-strain curve used to represent the material response to a cavitation impact, characterized by either its (a) impact load stress, as estimated by the average impact pressure or (b) stored energy.

In order to provide an improved physical link between multiphase flow predictions of cavitation cloud collapse and the resultant material response, the authors developed a new erosion metric premised on the fluid-solid energy transfer [13]. To represent the progressive damage to the material from repeated impacts, a cumulative stored energy by the material, E_{stored}, after N impacts can be calculated

$$E_{stored}(N) = \sum_{i=1}^{N} E_{impact,i} = \sum_{i=1}^{N} \frac{\mathcal{A}}{\rho_l c_l} \int_0^\tau p^2(t)dt. \tag{1}$$

The energy of a given impact, $E_{impact,i}$ is based on a pressure wave of magnitude p that propagates through a medium [14], characterized by its acoustic impedance (i.e. the product of its density ρ_l and speed of sound c_l), and acts on the surface of area $\mathcal{A}$ over a duration of time τ. For pressure amplitudes in excess of the material yield strength, the predicted impacts can be related to $E_{impact,i}$ via Equation 1. The cumulative predicted E_{stored} after numerous cavitation collapse events can then be used as a measure of the progress towards material rupture. By evaluating Equation 1, it is evident that the E_{stored} metric offers potential advantages over the MPDR approach in its ability to capture the influence of both impact stress and loading timescale on the predicted erosion potential. The authors found that E_{stored} was able to reliably indicate the critical erosion locations and relative erosion severity over a range of flow conditions [13].

The objective of this work is to extend the predictive capability of the stored energy erosion metric by deriving, implementing, and evaluating the relationship between E_{stored} and the erosion incubation period. The incubation period, T, is an important measure of erosion potential and severity as it quantifies the time before material rupture and has been shown to be inversely related to the steady material erosion rate [15]. In the first section of the paper, the theoretical relationship between E_{stored} and T is derived. This relationship is then assessed in a computational study of pressurized fuel through a simplified channel geometry [2], where the predicted distributions of peak impact pressures and E_{stored} are compared over a range of flow conditions. The measured T and critical erosion sites [2] are then compared with the predicted erosion parameters based on the MDPR and E_{stored} methods. Conclusions and major findings from this work are then summarized in the final section.

Experimental Data for Model Validation

Experimental data characterizing the flow of diesel fuel through a channel geometry from the work of Skoda et al. [2] are used to assess the cavitation predictions and erosion modeling approaches. A summary of the flow conditions evaluated in this study is provided in Table 1. In order to accelerate the measured cavitation erosion process, the channel was constructed out of aluminum, which is known to have a relatively low yield stress. Although the aluminum alloy used in the experiments was not specified, the properties of aluminum can be approximated as a bilinear material, where an elastic response occurs for stresses lower than the yield stress and plastic deformation results from stresses between the yield and ultimate stress. As such, for impact loads smaller than the yield stress, the material can be expected to respond elastically, where the material returns to its initial stress condition, and no damage occurs. For these experiments, a threshold for the impact stress is estimated as 60 MPa, based on reported yield stress specifications for aluminum 6082-O under static loading conditions [16].

Table 1. Summary of experimental conditions within the PREVERO Channel "I" Geometry.

Operating Point #	OP 6	OP 7	OP 8
Upstream Reservoir Pressure	20 MPa	30 MPa	40 MPa
Pressure drop across channel	12.5 MPa	17.5 MPa	22.5 MPa

Measured length of cavitation cavity (Percent of channel length)	91%	90%	65%
Measured critical erosion site (Percent of channel length)	No recorded erosion	72%	54%
Measured incubation period	No recorded erosion	60 min	30 min
Cavitation regime	Choked flow	Developing cavitation	Developing cavitation
Reynolds Number	1.52e05	1.80e05	2.05e05
$K = \dfrac{P_1 - P_v}{P_1 - P_2}$	1.598	1.713	1.777

Computational Model Set-Up

The commercially available CFD code CONVERGE [17] is utilized to model cavitation within the PREVERO Channel "I" geometry from the experimental work of Skoda et al. [2]. Erosion indicators were implemented into CONVERGE via a user-defined function (UDF), which allows for multiphase flow predictions to be related to progress towards material failure. The key parameters describing the fuel surrogate properties are summarized in Table 2. Diesel fuel is represented as a compressible barotropic fluid, using fluid properties for n-heptane and a reference liquid density of diesel fuel, based on measurements from Payri et al. (ρ_{ref} = 833.6 kg/m³ at P_{ref} = 30 MPa) [18]. The treatment of liquid-phase fuel as barotropic is justified based on findings from the work of Mihatsch and co-workers [11], who found that a barotropic assumption and a full thermodynamic treatment of the liquid yielded similar predictions of vapor cloud collapse. The flow is also assumed to be adiabatic. Together with the barotropic treatment of the fluid, the flow can be considered isothermal. The adiabatic assumption is a good one based on the Jakob number and residence time scale for the studied condition, which indicates that inertial effects, as opposed to interphase heat transfer, control bubble growth and collapse. Additionally, a trace amount of non-condensable gas is assumed to be present in the fuel, as represented with a given N₂ mass fraction, Y_{N2}, based on recommendations from Battistoni et al. [19].

Table 2. Thermodynamic and transport properties of diesel fuel surrogate modeled in this work.

Diesel fuel surrogate	Reference fuel density (ρ_{ref})	Reference pressure (P_{ref})	Fuel bulk modulus	Fuel temp.	Liquid fuel viscosity (T_{ref}=333K)	Fuel vapor pressure (P_v) (T_{ref}=333K)	Nitrogen mass fraction in fuel (Y_{N2})
n-heptane	833.6 kg/m³	30 MPa	1.90 GPa	333K	3.88e-04 Ns/m²	24.8 kPa	2e-05

An illustration of the Channel I geometry and simulated domain is shown in Figure 2. Key features of the channel geometry include a nominally constant diameter of 304 μm and a channel length of 995 μm. This geometry is of particular interest because of the increased propensity for flow separation and cavitation due to the sharp inlet corner. A portion of the central slice of the domain is shown in Figure 2 to highlight the computational mesh and employed levels of embedding. At runtime, the computational mesh is generated using a modified, cut-cell Cartesian method, where additional regions of refinement have been selected using fixed embedding. The base grid size, as can be seen in the inlet and outlet reservoirs, is 40 μm while 4 levels of fixed embedding are used to achieve minimum cell sizes of 2.50 μm to resolve the flow into the channel. In previous work by the authors, this level of grid resolution was found to yield grid converged results for the flowfield and cavitation predictions [20].
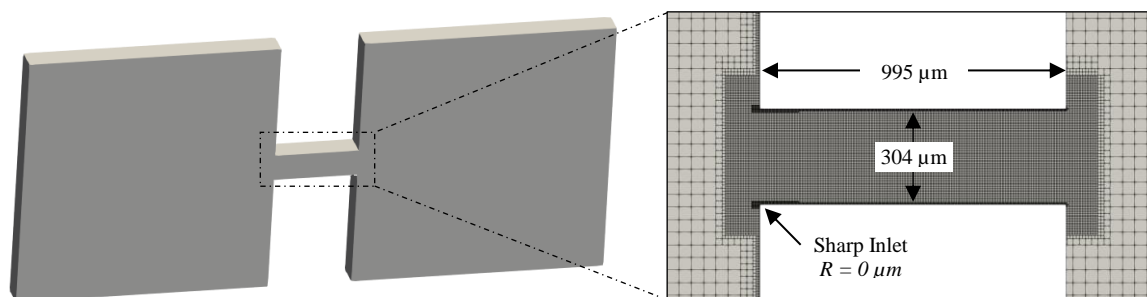

Figure 2. An illustration of the simulated domain, along with details of fixed embedding in channel geometry.

The cavitating flow within the channel is treated as a compressible, homogeneous, multi-phase mixture. The transient simulation methodology is based on the solution of the filtered Navier Stokes equations for a Large Eddy

Simulation (LES). Turbulence is accounted for using the dynamic structure model [21], while the wall shear stress is estimated using the Werner and Wengle wall model [22], which is based on analytical integration of the near wall velocity distribution. The flow within the channel is modeled as a single fluid comprised of three-components and two-phases, specifically liquid and vapor fuel and non-condensable gas, represented as N_2. Within the homogeneous mixture modeling approach, thermal and mechanical equilibrium are assumed, whereby all components are assumed to have the same pressure, temperature and velocity within a given computational cell. Using a pseudo-density concept, the mixture density, ρ, is calculated using volume-weighted averaging,

$$\rho = \sum_{i=1}^{3} \alpha_i \rho_i \tag{2}$$

where α_i and ρ_i are the void fraction and density of the ith-component, respectively. For gaseous phases, the density is determined using the Redlich-Kwong equation of state, whereas the liquid-phase density is determined using a barotropic relation for compressible liquids. Unlike standard volume of fluid (VOF) methods, α is not directly transported. Rather, α is determined via the species mass fraction, Y_i, of the ith-component, which is solved for in the species transport equations,

$$\frac{\partial \rho Y_i}{\partial t} + \nabla \cdot \rho Y_i \vec{v} = \nabla \cdot (\rho D \nabla Y_i) + S_i \tag{3}$$

where $\vec{v}$ and D are the velocity and diffusivity of the mixture, and S_i is the source term due to mass transfer (i.e., cavitation and condensation). Due to the adiabatic assumption employed to model the flow, solution of the energy equation for the mixture is omitted.

Cavitation and condensation are represented using the homogeneous relaxation model (HRM) [23], where the rate at which the instantaneous quality of fuel, x, approaches its equilibrium value, $\bar{x}$, is defined with the following relation,

$$\frac{Dx}{Dt} = \frac{\bar{x} - x}{\theta} \tag{4}$$

$$\theta = \theta_0 \alpha^{-0.54} \psi^{-1.76} \tag{5}$$

where θ is the relaxation time scale. For cavitation, the phase change timescale is set equal to θ, where θ_0 is a coefficient set to 3.84e-7, and ψ is the non-dimensional pressure ratio ($\psi = \frac{p_{sat} - p}{p_{crit} - p_{sat}}$). Although the presence of non-condensable gas is included in this model, no additional models are included to represent the adsorption and absorption of N_2. As a result, the mass transfer source term in the N_2 species transport equation is set to zero.

Relating Predicted Stored Energy to the Erosion Incubation Period

As previously discussed, using E_{stored} as a cavitation erosion metric provides an improved physical link between predicted cavitation collapse events and the resultant material response. By developing a theoretical relationship between E_{stored} and T, this erosion modeling approach can be used to quantify progress towards material erosion and be extended to predict the steady state material removal rate. Using the theory outlined in the work of Franc [12], it is possible to estimate the total energy required for the material to reach failure. After a single impact, the most superficial layer of the material surface behaves as schematically represented in Figure 1(a). For a given impact load of σ, the work per unit volume done on the most superficial layer is equal to the area under the stress-strain curve. For internal material layers, strain ($\varepsilon(z)$) along with absorbed energy decreases with distance, z, due to work hardening, which can be represented as follows,

$$\varepsilon(z) = \varepsilon_0 \left[1 - \frac{z}{l}\right]^\vartheta \tag{6}$$

where ε_0 is the strain at the surface, l is the thickness of the hardened layers and ϑ is a material-dependent shape factor. The thickness of hardened layers reaches a maximum, L, when the work-hardening process is complete. Typical values for an aluminum alloy, such as Al 7075, are $\vartheta = 2.0$ and $L = 690$ μm [15]. Using this information, the work done on the material by a given impact load σ can then be calculated with the following relation,

$$W(\epsilon_1) = \int_{z=0}^{L} \left[\int_{\epsilon=0}^{\epsilon=\epsilon_1} \sigma \, d\epsilon \right] \mathcal{A} \, dz, \tag{7}$$

where ε_1 is the strain associated with impact load σ acting on an area, $\mathcal{A}$. The total work, W_{total}, required for material failure can be computed when ε is set to the ultimate strain, ε_U, which marks the point of rupture. Because W_{total} is only dependent on material properties, it can be calculated to determine the erosion resistance of a given material. By relating E_{stored} to W_{total}, as schematically represented in Figure 1(b), it is possible to determine the erosive potential of hydrodynamic impacts. The ratio of W_{total} to E_{stored} represents the number of such impacts that would

be required to reach failure. Because E_{stored} quantifies the amount of energy absorbed by the material within a simulated timeframe, τ_{sim}, T can be estimated by relating T to the time required for the material to absorb an amount of energy equal to W_{total},

$$T \propto \frac{W_{total}}{E_{stored}} \tau_{sim}. \tag{8}$$

This relationship highlights several key influential factors on erosion severity. Firstly, a material with a high erosion resistance would be characterized by a large W_{total} value, and would result in a long incubation period. Additionally, flow conditions that produce highly erosive impacts would yield large E_{stored} values and short incubation periods. A similar relationship can be shown using the MDPR approach,

$$T \propto \frac{W_{total}}{W(\bar{\varepsilon})} \tau_{sim}. \tag{9}$$

where $\bar{\varepsilon}$ corresponds to the strain for a predicted average impact loading, $\bar{P}$. The key difference between Equations 8 and 9 is in how the cavitation impacts are related to the amount of energy absorbed by the material. As previously defined in Equation 1, E_{stored} is a function of the impact loading timescale, τ, which would yield a dependence of T on τ in Equation 8 that is not observed in the functional relationship in Equation 9. The effect of these differences on the predicted T and its response to changes in flow conditions will be discussed in the next section.

Results and Discussion

To verify the ability of the modeling approach to capture the thermofluidic conditions leading to cavitation erosion, predictions of mass flow rate at the channel entrance for a reservoir inlet pressure of 30 MPa, as defined for OP 7 condition, have previously been validated by the authors [20]. Comparison of predicted and measured mass flow rate exhibited excellent agreement, in terms of both the magnitude and the critical pressure drop condition leading to the onset of choked flow conditions. This validation exercise suggests that the fluid properties and treatment of the multiphase flow in this modeling approach well represent the experimental flow conditions at the channel entrance, and can be extended to other inlet pressure conditions, such as those for OP 6 and 8. The cavitation predictions are now compared with experimental time-averaged transmission images, which have been used as an indication of cavitation probability, as shown in Figure 3(a) for the OP 8 condition. To compare with the experimental transmission image, the predicted 3D total void fraction distribution is projected along the line of sight and time-averaged over a period of 250 µs after the flow has reached steady state in terms of mass flow rate. Under the OP 8 condition, a cavitation length of 60% of the channel length is predicted, as shown in Figure 3(b), which is in good agreement with the measured steady cavitation length of 65% of the channel length. Similar comparisons were conducted for the OP 6 and OP 7 conditions, although the dimensions of the cavitation cavity appear to be underpredicted relative to those indicated by the transmission image. For the lower inlet reservoir pressure conditions, the cavitation development is likely more sensitive to surface imperfections and deviations from the nominally specified geometry. As a result, the underpredicted cavitation lengths may be due to the exclusion of real geometry effects in the simulated geometry. Future investigations will evaluate the influence of surface roughness on the cavitation development under these operating conditions.
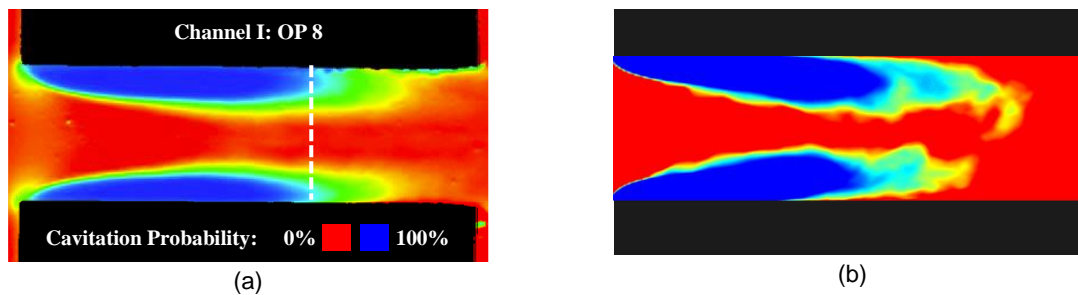

Figure 3. Comparison of (a) experimentally observed cavitation probability from Skoda et al. [2] with the (b) predicted projected total void fraction for cavitating flow through the Channel I geometry under the OP 8 condition.

To evaluate the model's ability to capture erosion propensity and severity, predicted distributions of the peak pressure and stored energy recorded on the bottom surface of the channel are compared with the experimentally measured critical erosion sites, as listed in Table 1. Visualizations of the accumulated peak pressure and stored energy distributions for the OP 8 condition are shown in Figure 4(a) and (b), respectively, after 348 µs of simulated time. For this particular condition, peak impact loads in excess of 400 MPa are observed in the middle of the channel. Similar locations are indicated by the predicted stored energy, where isolated high load impacts result in large impact energies. However, it is important to highlight regions, such as the one indicated within the dotted ellipse, where relatively lower impact loads can result in substantial stored energy in the material due to the impact

duration. Accumulated stored energy in excess of 50 nJ after 348 μs of operation can be seen in the middle of the channel.
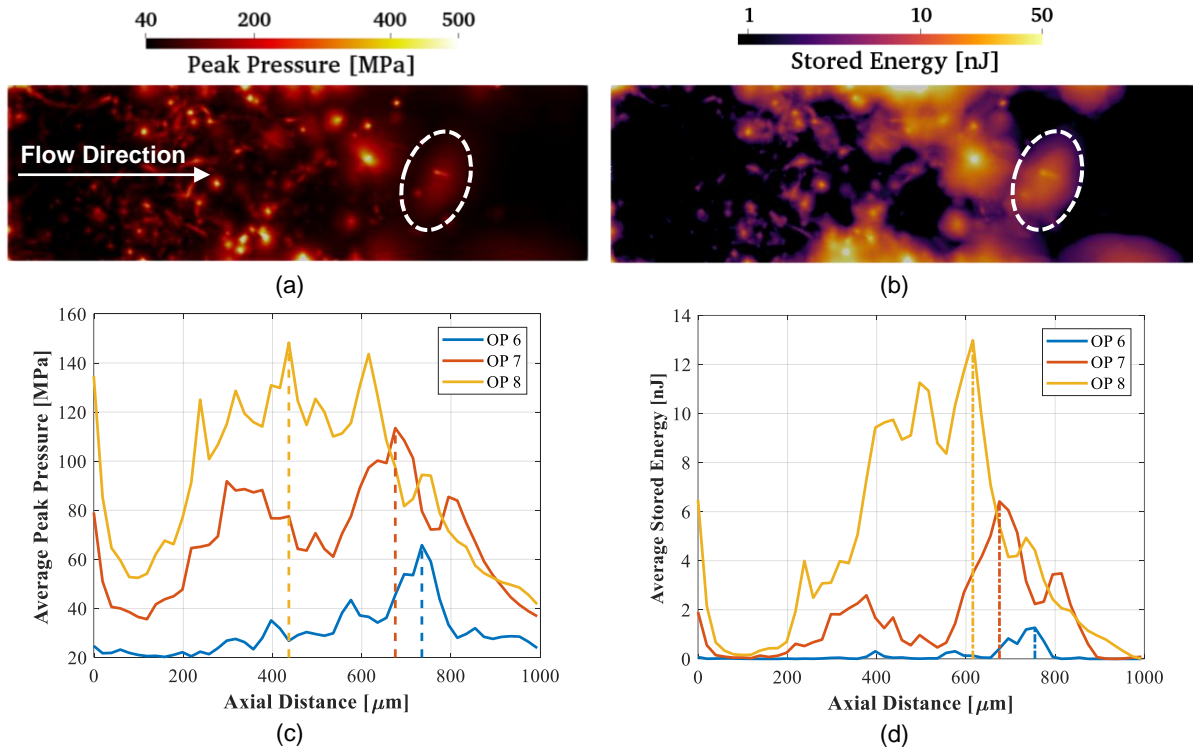

(a)

(b)

(c)

(d)

Figure 4. Visualization of the predicted (a) peak pressure and (b) stored energy distributions along the bottom of the channel under the simulated OP 8 condition after 348 μs of simulated time. Comparison of the axial distributions of (c) peak pressure and (d) stored energy predictions, which have been averaged across the width of the channel, for all three evaluated conditions.

To better characterize the cavitation collapse impacts throughout the channel, axial distributions of the peak pressure and stored energy averaged across the width of the channel were calculated. The axial distributions can be seen in Figure 4(c) and (d) for average peak pressure and stored energy, respectively. In general, the average peak pressure and stored energy are observed to increase as the Reynolds number, *Re*, increases from the OP 6 to OP 8 condition. By identifying the maximum in these distributions, as indicated by the dashed lines in Figure 4(c) and (d), it is possible to identify the critical axial locations where cavitation erosion is likely to occur first. Both the average peak pressure and stored energy indicate that the critical location can be found further upstream with increasing *Re* and cavitation number, *K*. However, the locations that are indicated by the stored energy distribution are found to be in better agreement with the experimental data, listed in Table 1, where the critical erosion sites are predicted to occur at 76%, 68%, and 61% of the channel length at the OP 6, OP 7 and OP 8 conditions.
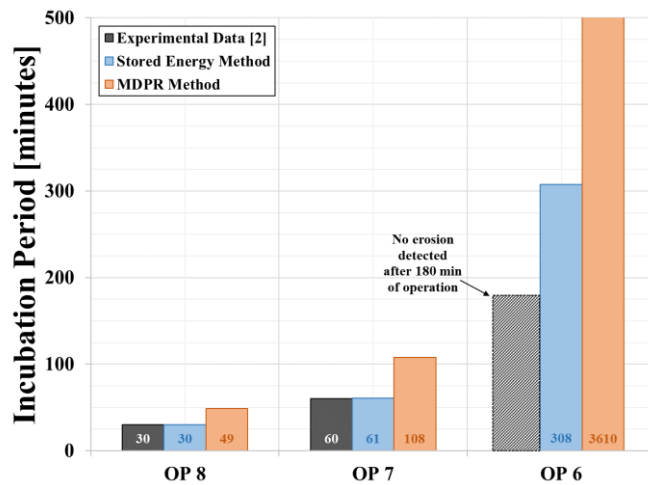

Figure 5. Comparison of the measured erosion incubation periods [2], *T*, against the predicted *T* using the stored energy- and MDPR-based methods across the range of flow conditions considered.

Using the predicted maximum values at the critical erosion sites from the average peak pressure and stored energy distributions, the incubation period can be calculated using Equations 9 and 8, respectively. A comparison of the measured and predicted *T* across the three flow conditions is shown in Figure 5. For the OP 8 and OP 7 conditions, the incubation periods were experimentally observed to occur at 30 and 60 minutes, respectively. For the OP 6 condition, no erosion was detected within the 180 minutes of operation. Across the range of operating conditions, both the MDPR and stored energy based approaches predict the correct trend of increasing erosion severity with *Re* and *K* from OP 6 to OP 8. It is clear from Figure 5 that the stored energy metric more accurately represents the sensitivity of *T* to the change in flow conditions from OP 8 to OP 7, as indicated by the agreement of the model predictions within 2% of the experimentally measured *T*. When the MDPR-based approach is used to estimate *T*, the erosion severity is underpredicted as indicated by the relatively larger *T*. Although both approaches predict incubation periods in excess of 180 minutes for the OP 6 condition, the sensitivity of *T* to the change in flow conditions from OP 7 to OP 6 conditions are drastically different. For the stored energy approach, the incubation period is predicted to increase by a factor of 5, whereas for the MDPR-based approach, the incubation period is predicted to increase by a factor of 33.

These differences in the predicted *T* across the range of flow conditions evaluated in this work have an appreciable impact on the ability to accurately predict erosion aggressiveness. As previously noted, the steady state material removal rate following the incubation period has been shown to be inversely related to the incubation period [15]. Therefore, MDPR-based approaches may not be suitable in predicting the erosion potential or steady state erosion rate. The findings from this study highlight the promise of the stored energy approach in capturing the sensitivity of erosion severity to changing flow conditions. Future studies will focus on the ability of the stored energy approach to predict erosion for different geometries, such as the PREVERO Channel "K" geometry [2] and practical injector geometries [1], and across a wider range of flow conditions where experimental data is available.

Conclusions

In order to extend the predictive capability of the stored energy, E_{stored}, erosion metric to represent the progress towards material failure and erosion severity, a relationship between E_{stored} and the incubation period, *T*, was derived and implemented into the CONVERGE CFD code. Comparison of the erosion predictions from the stored energy approach and the commonly employed mean depth penetration rate (MDPR) method with available experimental data for critical erosion sites and *T* revealed the following findings:

- While the MDPR-based approach is able to capture the influence of material properties on erosion progress, it is unable to capture the effect of loading timescale on the cavitation impact strength. In contrast, the stored energy method allows for a more accurate treatment of the cavitation collapse event by considering both the impact load and duration.
- The stored energy distribution was better able to represent the critical erosion sites relative to the peak impact pressure distribution, and the response of these locations to changes in the flow conditions.
- For the range of evaluated conditions, the stored energy approach was able to predict the correct sensitivity of *T* to changes in the flow conditions. Overall, the MDPR approach was found to underpredict the erosion severity.

To extend the rigor of validation for the stored energy approach, future investigations will focus on cavitation and erosion predictions under a wider range of flow conditions and within different geometries of interest, such as the PREVERO Channel "K" geometry with a rounded inlet to the channel and practical fuel injector geometries.

Acknowledgements

Nomenclature

$\mathcal{A}$ impact area [m^2]
α   void fraction [-]
ε   strain of a given impact load [-]
θ   phase change timescale [s]
ϑ work-hardening shape factor [-]
ρ$_l$ liquid-phase density [kg/m^3]

σ	stress of a given impact load [Pa]
τ	impact load timescale [s]
τ_{sim}	simulated time period [s]
ψ	pressure ratio [-]
c_l	liquid-phase speed of sound [m/s]
D	mixture diffusivity [m^2/s]
E_{stored}	stored energy by the material from several cavitation impacts [J]
K	cavitation number [-]
l	depth of work-hardened layers [m]
L	maximum depth of work-hardened layers [m]
p	impact pressure [Pa]
$\bar{P}$	mean impact pressure [Pa]
Re	Reynolds number [-]
T	erosion incubation period [s]
T_{ref}	reference fuel temperature [K]
W	work done on the solid material by a given cavitation impact [J]
W_{total}	total work required for solid material failure [J]
x	mixture quality [-]
Y_i	mass fraction of ith species [-]
z	depth within solid material [m]
HRM	homogeneous relaxation model
LES	large eddy simulation
OP	operating point
MDPR	mean depth penetration rate

References

1. Tzanatekis, T. et al., April 9-11 2019, SAE World Congress.
2. Skoda, R., Iben, U., Morozov, A., Mihatsch, M., Schmidt, S., Adams, N., July 4-6 2011, WIMRC 3rd International Cavitation Forum.
3. Hattori, S., Mori, H., Okada, T., 1998, Journal of Fluids Engineering, 120 (1), pp. 179-185.
4. Dular, M., Petkovšek, M., 2015, Experimental Thermal and Fluid Science, 68 (1), pp. 359-370.
5. Winklhofer, E., Kull, E., Kelz, E., Morozov, A., Sept. 2-6 2001, 17th Annual Conference on Liquid Atomization & Spray Systems (ILASS-Europe).
6. Mitroglou, N., Stamboliyski, V., Karathanassis, I.K., Nikas, K.S., Gavaises, M., 2017, Experimental Thermal and Fluid Science, 84 (1): pp. 179-189.
7. Gavaises, M., Papoulias, D., Andriotis, A., Giannadakis, E., Theodorakakos, A., 2007, SAE Technical Paper 2007-01-0246.
8. Koukouvinis, P., Karathanassis, I.K., Gavaises, M., 2017, International Journal of Engine Research, 19 (3): pp. 360-373.
9. Koukouvinis, P., Gavaises, M., Li, J., Wang, L, Dec 6-10 2015, 9th International Symposium on Cavitation.
10. Brusiani, F., Falfari, S., Bianchi, G.M., 2015, Energy Procedia, 81 (1): pp. 755-764.
11. Mihatsch, M.S., Schmidt, S.J., and Adams, N.A., 2015, Physics of Fluids, 27 (10): pp. 103302:1-21.
12. Franc, J.-P., 2009, Journal of Fluids Engineering, 131 (2), pp. 021303-021303-14.
13. Magnotti, G.M., Battistoni, M., Saha, K., Som, S., July 22-26 2018, 14th Triennial International Conference on Liquid Atomization and Spray Systems.
14. Landau, L.D., and Lifshitz, E.M., 1987, "Fluid Mechanics."
15. Kim, K.-H., Chahine, G., Franc, J.-P., and Karimi, A., 2016, "Advanced experimental and numerical techniques for cavitation erosion prediction."
16. Society of Automotive Engineers and American Society for Testing and Materials, 1999, "Metals and Alloys in the Unified Numbering System."
17. Richards, K.J., Senecal, P.K., Pomraning, E., 2018, "CONVERGE 2.3 Manual."
18. Payri, R., Salvador, F.J., Gimeno, J., Bracho, G, 2011, Fuel, 90 (3): pp. 1172-1180.
19. Battistoni, M., Duke, D., Swantek, A.B., Tilocco, F.Z., Powell, C.F., Som, S., 2015, Atomization and Sprays, 25 (6): pp. 453-483.
20. Magnotti, G.M., Battistoni, M., Saha, K., Som, S., April 9-11 2019, SAE World Congress.
21. Pomraning, E., 2000, "Development of Large Eddy Simulation Turbulence Models."
22. Werner, H., Wengle, H., 1993, "Turbulent Shear Flows".
23. Bilicki, Z., Kestin, J., 1990, Proc. R. Soc. Lond. A., 428: pp. 379-397.